ISSN 0010-9525, Cosmic Research, 2020, Vol. 58, No. 3, pp. 139–149. © Pleiades Publishing, Ltd., 2020.
Russian Text © The Author(s), 2020, published in Kosmicheskie Issledovaniya, 2020, Vol. 58, No. 3, pp. 179–190.

Association of Inclined Sporadic *E*-Layers and Small-Scale Atmospheric Waves in Earth's Ionosphere

V. N. Gubenko[a], * and I. A. Kirillovich[a]

[a] *Kotelnikov Institute of Radio Engineering and Electronics, Russian Academy of Sciences, Fryazino, 125009 Russia*

**e-mail: vngubenko@gmail.com*

Received February 20, 2019; revised August 5, 2019; accepted October 23, 2019

Abstract—A new method has been developed for determining the characteristics of internal atmospheric waves based on the use of inclined sporadic *E*-layers of Earth's ionosphere as a detector. The method is based on the fact that an internal wave, propagating through an initially horizontal sporadic *E*-layer, causes rotation of the plasma density gradient in the direction of the wave vector, which leads to the establishment of a layer ionization plane parallel to the phase wave front. The developed method allows us to study the relationship between small-scale internal waves and sporadic *E*-layers in Earth's ionosphere and significantly expands the capabilities of traditional radio occultation monitoring of the atmosphere. It was found that the studied internal atmospheric waves have periods from 35 to 46 min and vertical phase velocities from 1.2 to 2.0 m/s, which is in good agreement with the results of independent experiments and modeling data for sporadic *E*-structures at an altitude of ~100 km in Earth's polar cap.

DOI: 10.1134/S0010952520030028

1. INTRODUCTION

Sporadic *E*-layers (E_s) are known as thin layers of increased ionization at altitudes from 90 to 130 km in Earth's ionosphere. The study of the effects associated with E_s-layers is of great interest for radio communications and navigation. Analyzing the radio occultation measurements of the *Challenging Minisatellite Payload* (*CHAMP*), the authors in [1] studied the global morphology of E_s-layers. The climatology of sporadic *E*-layers was studied by them on the basis of determining the signal to noise ratio (SNR) and phase dispersions, in terms of monthly zonal averages, seasonal maps, and daily and long-term variations [1]. A detailed analysis of the global distribution of the appearance of sporadic *E*-layers was carried out in [2]. To obtain information on small-scale ionospheric inhomogeneities for the period from January 2002 to December 2007, the authors of this paper used a large database of radio occultation missions *CHAMP*, *GRACE*, and *FORMOSAT-3/COSMIC*. It was found that the distribution of the appearance of E_s-layers shows strong fluctuations, though the highest frequencies of their occurrence are observed during the summer at middle latitudes. Maxima of the appearance of inhomogeneities arise in the range of geomagnetic latitudes from 10° to 60° of the Earth's middle latitude ionosphere. At high latitudes, where the angles of magnetic inclination are from 70° to 80°, deep minima occur in the indicated distribution, which is consistent with the theory of the formation of sporadic layers using wind shear [2, 3].

The theory of the formation of sporadic *E*-layers by means of a wind shear at middle latitudes has been confirmed by many studies [4]. It was found that E_s-layers at middle latitudes are very thin (several hundred meters thick), distributed horizontally over hundreds of kilometers, dense (particle concentration reaches several units of 10^6 electrons/ions per cm^3), and composed of metal atoms [5]. In the presence of inclined geomagnetic fields, ion fusion in the *E*-region of the ionosphere can be due to a shear by both zonal and meridional winds. However, the main driver of ion convergence in middle latitudes at an altitude of ~115 km and lower is considered to be a shear of the zonal wind [6]. Electrons associated with the process of fusion of positive ions into a thin layer move along the lines of the geomagnetic field in order to neutralize the positive charge. It should be noted that the theory of wind shear explains how a layer is formed in the vertical plane but does not explain the principle of horizontal formation. In the daytime *E*-region of the ionosphere, the main molecules for ionization are N_2 and O_2. At night, the fast recombination of molecules leads to the photochemical equilibrium of ionization in the *E*-region, which causes the disappearance of the usual *E*-layer. On the other hand, sporadic *E*-layers are often observed at night and their appearance usually lasts several hours. This contradicts the photochemical equilibrium of the usual *E*-region of the ionosphere and excludes its participation as a possible source of positive ions responsible for the ionization of E_s-layers. To confirm the assumption that it is metal ions (Fe^+ and Mg^+) are the main source of ionization of E_s-layers, the profiles of

the concentration of electrons and ions were directly measured using rocket observations [7]. The theory predicts that the recombination rates for these metal ions are significantly lower than the corresponding values for NO^+ and O_2^+. The lifetime of metal ions is long and varies from several days at an altitude of ~120 km to several hours at an altitude of ~95 km [6]. It is very likely that metal atoms came from a meteor, therefore it is natural to assume that the formation of thin layers is associated with the convergence of ions, which is caused by the impact of neutral wind in the presence of a geomagnetic field. Although in some observations of powerful E_s-layers, meteors are found captured at the nodes of the wind shear, however, the main mechanisms of the formation of sporadic layers are considered to be neutral wind shears [8–10].

Ground-based radar observations at night made it possible to successfully represent the horizontal structure of E_s-layers [11–13]. Numerical modeling showed that E_s-spots (layers) in the northern hemisphere are propagated towards the southwest and, as a rule, are elongated in the (NW-SE) direction from the northwest to the southeast [14–16]. However, in order to justify the simulation results, it is necessary to have a larger number of observations of sporadic E-layers at middle latitudes. In the presence of vertical wind shear, the main mechanisms of structuring E_s-layers are: internal gravity waves (IGWs) [17–19], shear instability of the neutral wind [13, 20–22], and plasma instability of the layer due to a neutral wind shear [14, 15]. Internal atmospheric waves modulate E_s-layers in the vertical direction, and they can cause quasiperiodic (QP) radar echo signals. It was shown in [23] that, as a result of modulation of the layers over altitude, the polarization electric field develops in the night ionosphere of middle latitudes, in this case, the effects of polarization resemble atmospheric waves in their effect. The deployment of coherent scattering radars in modern ionospheric experiments provided a clear picture of structuring of ionization layers for middle latitudes [24, 25]. Rocket experiments showed that quasiperiodic echo signals emanate from sporadic E-layers, in this case, the presence of strong electric polarization fields and neutral wind shears is observed [26, 27]. Large wind shears did indeed take place in two rocket experiments, which were carried out in parallel with ground-based radar studies (SEEK and SEEK-2) of sporadic E-layers in the ionosphere above Kyushu island [28–30]. Shear instability in a neutral atmosphere is also considered as a mechanism for creating a densely ionized billow structure [21]. In the upper part of the rocket experiment conducted during the SEEK-2 mission, this billow structure in the E-region of the ionosphere was represented as a trace of trimethylaluminum (TMA) [29]. Observations of the three-dimensional structure of downward and approaching echo signals [31] can be explained by the presence of unstable regions that developed along the geomagnetic field line from the altitudes of the E_s-layer location to higher levels (>120 km). The data of interferometric measurements obtained in [31] support the model proposed in [32, 33] and confirm the results of computer simulation [34].

The mechanism of the formation of E_s-layers by means of a wind shear at high latitudes (>60°) will not be as effective as at middle latitudes due to the fact that, here, the magnetic field is directed almost vertically to the local horizon. The large-scale horizontal plasma structure in the auroral E-region is determined by the spatial distributions of solar radiation sources and particle precipitation. Internal atmospheric waves at high latitudes are less important as a mechanism for the vertical structuring of layers due to the large angle of inclination (~90°) of the magnetic field to the local horizon [35]. However, the small angle of deviation of the magnetic field from vertical is very significant due to large electric fields directed perpendicular to the magnetic field. At high latitudes, convective electric fields are important drivers of convergence or divergence of ion motion [5, 36–41]. The authors in [36] first suggested that sporadic E-layers at high latitudes can be formed as a result of the action of only one electric field, where the wind shear mechanism practically does not operate, in particular at altitudes below 110 km. Compared to the equatorial region, the electric field in the aurora zone and the polar cap is noticeably larger and more widely distributed over the area. The average auroral electric field has a strong diurnal component with an amplitude of 30 mV/m and with maxima located near 05.00 and 18.00 local time. The field strength of ~50 mV/m is usual for both the oval and the polar cap. Numerous measurements have also been reported, in which the magnitude of the electric field exceeded the value of 100 mV/m [35]. Clear signatures of the influence of tidal winds (semidiurnal and diurnal modes) on the formation of sporadic layers (electric fields are not considered) are observed, however, internal atmospheric waves can also create additional wind nodes [37]. In fact, the authors in [42] showed that under very quiet conditions of auroral latitudes, the presence of minimal electric fields is sufficient for the formation of a sporadic E-layer using a wind shear. Evidence was presented in [43] that E_s-concentrations of $\sim 3 \cdot 10^6$ cm^{-3} are often observed at high latitudes, and there is also a sufficient amount of Na^+ ions to obtain experimentally measured concentrations of Na atoms. The composition of metal ions in E_s-layers suggests their association with the processes of ablation of meteors [44], as well as with the formation of neutral metal layers in the upper mesosphere [40, 41, 45]. Since the vertical velocity is proportional to the cosine of the angle of inclination of the magnetic field to the local horizon, which becomes equal to 0.034 for the angle of inclination of 88°, which is significantly less than 0.17 for the angle of 80° [35], mechanisms involving horizontal electric fields or neutral winds will not

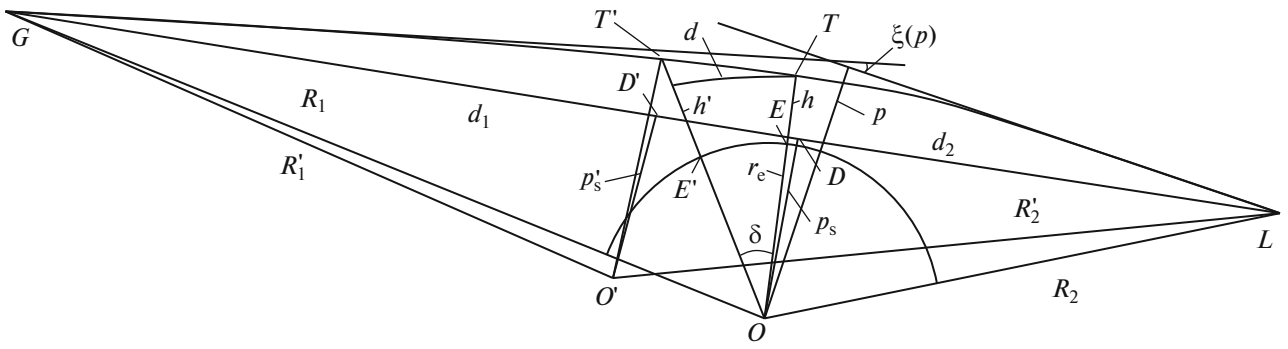

Fig. 1. Scheme of the radio occultation experiment in Earth's ionosphere.

operate in the polar cap. It is assumed that high-latitude E_s-layers can be a manifestation of auroras that correspond to the region of increased ionization. However, the sporadic layers produced in this case will not be too thin. According to the results of [5], at high latitudes there are several types of layers that are much thinner than those caused by auroral precipitations, and which are probably formed for reasons characteristic of sporadic *E*-layers at middle latitudes.

The propagation of a small-scale IGW modulates the structure of the initially horizontal E_s-layer, which leads to the inclination of this layer relative to the plane of the local horizon. We have developed a method for determining the characteristics of internal atmospheric waves based on the use of inclined sporadic layers of Earth's ionosphere as a detector. The goal of this study is: (I) to present a method for determining the localization and inclination of plasma sheets from radio occultation data; (II) conducting a study for the case of inclined sporadic *E*-layers in Earth's high-latitude ionosphere, observed using the *CHAMP* satellite; and (III) demonstrating a new method for determining IGW characteristics, which determine the inclinations of the studied E_s-layers.

2. METHOD FOR DETERMINING THE POSITION OF PLASMA LAYERS AND THEIR INCLINATIONS TO THE LOCAL HORIZON BY RADIO OCCULTATION DATA

The scheme of the radio occultation experiment is shown in Fig. 1. Highly stable radio signals emitted by a transmitter located on navigational satellite *G* pass through the ionosphere and atmosphere along the *GTL* beam and are recorded by the receiver aboard low-orbit satellite *L*. Measurements of amplitude $A(t)$ and the phase-path increase (eikonal) $\Phi(t)$ are carried out on a carrier frequency as a function of time *t*. The global spherical symmetry of the ionosphere and atmosphere with a common center (point *O* in Fig. 1) is a key assumption in the analysis of radio occultation data. The main contribution to variations in the amplitude and phase of the recorded signal is made by a small region near tangential point *T*, where the radio beam is perpendicular to the gradient of the refractive index, despite the fact that the length of beam trajectory *GTL* is much longer than the region length [46]. The length of this region on the beam trajectory is $\Delta_h = 2(2l_f r_e)^{1/2}$ and it is equal to the horizontal resolution of the structure under study in a radio occultation experiment. Here, $l_f = (\lambda d_2)^{1/2}$ is the vertical size (radius) of the Fresnel zone, λ is the wavelength of the radio signal, r_e is distance *OT* from center *O* of the spherical symmetry of the medium to perigee of the beam *T*, and d_2 is the length of the section of beam trajectory *TL*, which is approximately equal to the length of straight segment *DL* (Fig. 1). Δ_h corresponds to the minimum length of a horizontal layer that can be measured by the radio occultation method. The tangential point, at which radio beam *GTL* is perpendicular to the gradient of the refractive index, coincides with the perigee of beam *T* providing global spherical symmetry. The radio occultation method makes it possible to determine the refractive index and its vertical gradient along the trajectory of the beam perigee with good accuracy and high vertical resolution.

An important relation between the acceleration of eikonal *a* and refractive attenuation $X_p(t)$ of the radio occultation signal has the form [47–49]:

$$1 - X_p(t) = ma, \quad a = d^2\Phi(t)/dt^2,$$
$$m = d_1 d_2/(R_0^{1/2} dp_s/dt)^2, \quad d_1 = R_0 - d_2, \tag{1}$$

where d_1, d_2, and R_0 are the lengths of straight segments *GD*, *DL,* and *GDL*, respectively, and *p* and p_s are the impact parameters for beam trajectory *GTL* and line of sight *GDL*. The value of *m* is determined from ballistic data for satellites. Since angle of refraction $\xi(p)$ (Fig. 1) is small, distance d_2 is approximately equal to the length of beam arc *TL*.

We formulate a criterion, under which the tangential point coincides with the beam perigee. For this, it is necessary and sufficient: (I) the fulfillment of the condition for global spherical symmetry of the atmosphere and ionosphere and (II) the absence of random

inhomogeneities and multibeam propagation of radio waves. In this case, Eq. (1) is valid, which leads to the identity of refractive attenuations of X_a and X_p determined from the amplitude and phase measurements of the radio occultation signal:

$$X_p(t) \equiv X_a(t), \quad X_a(t) = I/I_0, \tag{2}$$

where I_0 and I are the intensities of the radio waves recorded before and after the beam enters the ionosphere, respectively. Identity (2) is a mathematical expression of the fact that the tangential point of the ionospheric layer coincides with the perigee of beam T. It is convenient to present the refractive attenuations of $X_p(t)$ and $X_a(t)$ determined from the measurements of the eikonal and amplitude of the radio occultation signal in the form of analytical functions with amplitudes $A_p(t)$ and $A_a(t)$ and phases $\chi_p(t)$ and $\chi_a(t)$:

$$\begin{aligned} 1 - X_p(t) &= ma = A_p(t)\,\mathrm{Re}\exp[j\chi_p(t)], \\ 1 - X_a(t) &= ma = A_a(t)\,\mathrm{Re}\exp[j\chi_a(t)]. \end{aligned} \tag{3}$$

Indicated amplitudes $A_p(t)$ and $A_a(t)$ and phases $\chi_p(t)$ and $\chi_a(t)$ can be found using known time dependence $1 - X_p(t)$ and $1 - X_a(t)$, for example, using numerical Hilbert transform or other methods for processing experimental data. In the case of synchronous variations $1 - X_p(t)$ and $1 - X_a(t)$, from Eq. (1) we can obtain:

$$A_p(t) = A_a(t), \quad \chi_p(t) = \chi_a(t). \tag{4}$$

Under the condition of global spherical symmetry, Eq. (4) is another form of the above criterion. Deviations from it can be associated with multibeam propagation, diffraction, scattering, as well as the influence of turbulence and other inhomogeneities in the atmosphere and ionosphere. In some cases, these deviations are caused by the influence of horizontal gradients and the appearance of other tangential points in the ionospheric sections of the radio beam, for example, tangential point T', which leads to a displacement of the center of spherical symmetry from point O to point O' (Fig. 1).

The ratio for determining the displacement d of tangential point T' relative to the perigee of beam T has the following form [48–50]:

$$d = d_2 \frac{A_a - A_p}{A_p}, \quad d_2 = \sqrt{R_2^2 - p_s^2}. \tag{5}$$

Equation (5) establishes the following rule: the displacement of the tangential (turning) point of the beam trajectory is determined from the relation between amplitudes A_a and A_p, which can be obtained from the analysis of variations in the intensity and eikonal of the radio occultation signal. Displacement d is positive or negative, depending on the sign of the difference $(A_a - A_p)$, and tangential point T' is located in GT or TL of the beam trajectory, respectively. In this case, phases $\chi_p(t)$ and $\chi_a(t)$ should be the same within the accuracy determined by the measurement errors. Equation (5) is valid, if one of the satellites is located at a much greater distance from the point of perigee T than the other satellite. This condition is fulfilled in radio occultation experiments, where spacecraft–Earth communication lines are used, or when low-orbit satellites operate with radio signals from space navigation systems. If displacement d is known, then we can determine correction Δh to calculate the actual layer altitude (h') and find the angle of inclination of layer δ to the local horizon [50]:

$$\delta = d/r_e, \quad \Delta h = h' - h = d\delta/2 = d^2/(2r_e), \tag{6}$$

where h is the altitude of the perigee beam (Fig. 1).

3. ANALYSIS OF *CHAMP/GPS* RADIO OCCULTATION DATA IN EARTH'S IONOSPHERE

We used the radio occultation measurements of the *CHAMP* satellite to study sporadic *E*-layers in Earth's ionosphere. Figure 2 shows the results of determining the position and inclination of the ionospheric layers using the data of processing radio signals at a frequency of 1575.42 MHz of the global positioning system (session on July 28, 2003, 01.35 UT (21.08 LT); beam perigee coordinates 71.4° N, 67.3° W). The parameters of ionospheric structures were determined based on the analysis of altitudinal variations of the phase path and the intensity of the radio occultation signal. This made it possible to estimate the spatial displacement of plasma structures relative to the perigee of the radio beam, to determine the angles of inclination of the layers to the local horizon, as well as to find the altitudes of the true location of the layers.

The time resolution of the phase and intensity measurements of the radio signal received at the *CHAMP* satellite is 0.02 s, which corresponds to the discretization frequency of 50 Hz. The analyzed data showed the presence of significant quasiregular variations in the intensity and phase of radio waves. The refractive attenuations of X_a and X_p of the radio occultation signal obtained as a result of processing variations in intensity and eikonal are shown in Fig. 2-I (curves *1* and *2*) as function of perigee altitude h of beam trajectory GTL. The refractive attenuation of X_p was found from Eq. (1) by using the values of parameter a determined from the experimental data. The value of m was calculated using satellite ballistic data. We found the refractive attenuation of X_a from measurements of the intensity of the radio occultation signal aboard the *CHAMP* satellite.

Variations of refractive attenuations of X_a and X_p are coherent, which indicates the equality of phases χ_a and χ_p. Obviously, the indicated variations in X_a and X_p are due to the influence of ionospheric layers in three intervals of the perigee altitude of beam trajectory GTL, which are indicated as a, b, and c in Fig. 2-I. The inter-

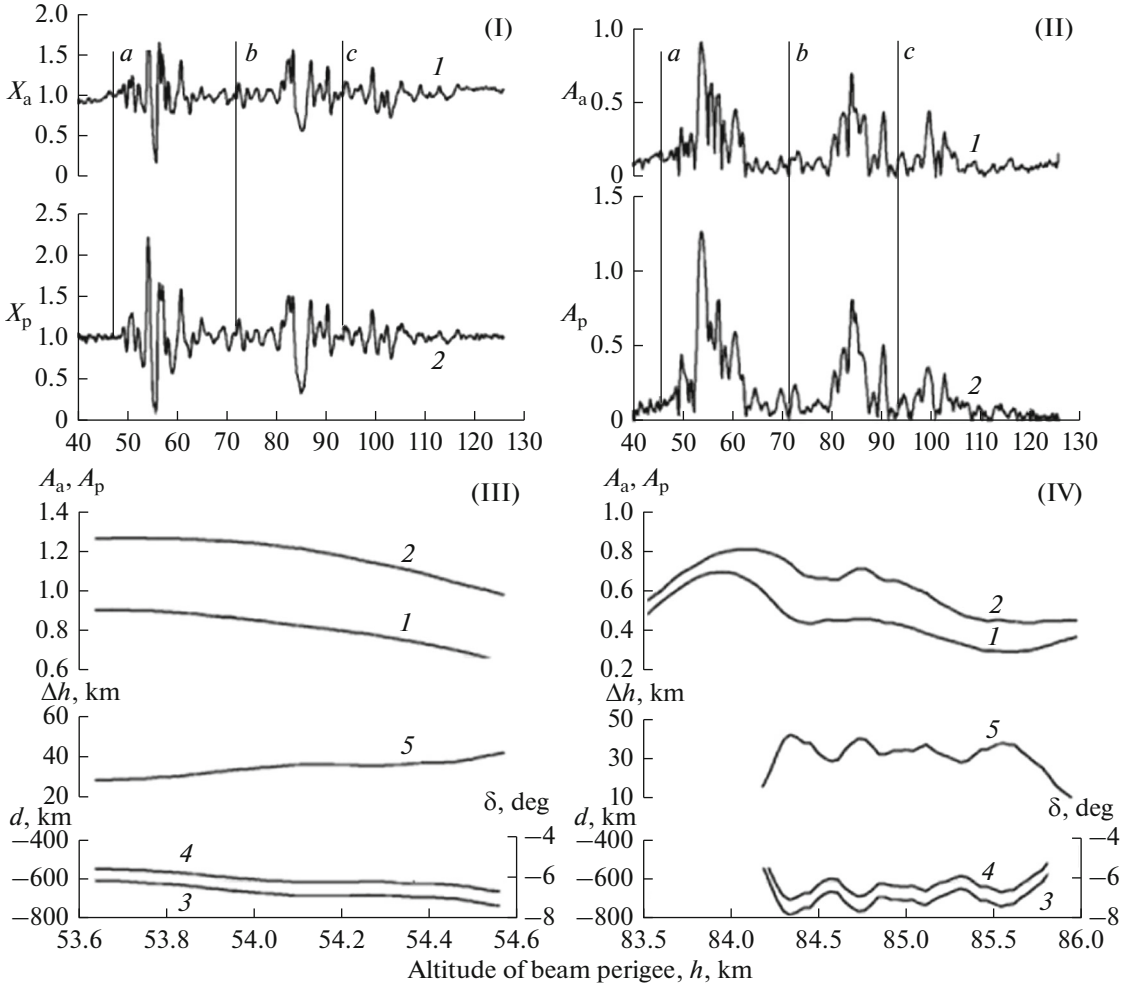

Fig. 2. Comparison of refractive attenuations of X_a and X_p obtained from variations in the intensity and eikonal of the radio occultation signal of *CHAMP* at the *GPS*-frequency f_1 = 1575.42 MHz (curves *1* and *2* in panel I, respectively). Amplitudes A_a and A_p of the analytical signals associated with variations in refractive attenuations of X_a and X_p (curves *1* and *2* in panel II, respectively). Position and inclination for the first (*a*) layer are determined by using the amplitudes A_a and A_p (panel III). Position and inclination for the second (*b*) layer are determined based on comparison of amplitudes A_a and A_p (panel IV).

vals *a*, *b*, and *c* correspond to the ranges of the beam perigee altitude: 50–72 km, 72–92 km, and 92–116 km, respectively. It can be seen that functions $(X_a - 1)$ and $(X_p - 1)$ are coherent in the indicated intervals. However, the amplitudes A_a and A_p of the analytic functions $(X_a - 1)$ and $(X_p - 1)$ are different. These amplitudes A_a and A_p were determined using the Hilbert numerical transform and they are shown in Fig. 2-II (curves *1* and *2*, respectively). The maximum values of parameter A_a are smaller than the corresponding values of A_p in intervals *a* and *b* (Fig. 2-II). The opposite picture is observed in interval *c* (Figs. 2-I and 2-II). For layers located in intervals *a* and *b*, the values of displacement *d* are negative. These two layers are located on the trajectory of the *GTL* beam between points *T* and *L*. The upper layer from interval *c* is displaced from the perigee of beam *T* towards navigational satellite *G* (Fig. 1). For the case of nonzero displacement of the layer, the values of actual layer altitude *h*' and the altitude of beam perigee *h* are not equal to each other and will differ by value Δ*h* determined from Eq. (6). It is important to note that the vertical position of the layer is not determined unambiguously by the value of beam perigee altitude *h*. For example, in accordance with Eq. (6), two layers with the same beam perigee altitude *h* and different values of displacement *d* will have different actual altitudes *h*'. Therefore, the actual altitude of the layer is a more suitable parameter for describing the altitude position of the layer compared with the altitude of the beam perigee.

Radio occultation studies have shown that in Earth's ionosphere not only discrete (single) sporadic *E*-layers are observed, but also more complex structures, such as double E_s-peaks and even rectangular sporadic layers [51]. Complex E_s-layers can be due to unstable wind shears. The authors of [21] argue that

drivers causing plasma instability (for example, Kelvin – Helmholtz instability) could deform a discrete E_s-layer into a complex structure. These drivers can raise part of the sporadic E-layer to overlap with the original layer [51]. As can be seen in Fig. 2-I, the layer in interval *a* has a complex (double) quasiperiodic structure. It is possible that the vertical observed oscillations are a sign of propagation through the layer of the IGW. The bottom part of this layer refers to the beam perigee altitude of 55 km and has a vertical size of 3.0 km, and its top part refers to the perigee height of 59 km and has a vertical size of 4.4 km. A single sporadic *b*-layer referred to the beam perigee altitude of 85 km, has a vertical size of 4.4 km, and a typical *U*-shaped structure, which was reported in [52], with oscillations above and below the defocusing region due to interference of the direct and refracted radio beams. The layer from interval *c* refers to the altitude of beam perigee of 103 km and has a vertical size of 3.0 km. Figure 2-I shows that this layer is less pronounced than the layers located in intervals *a* and *b*.

Since the variations in refractive attenuations of X_a and X_p are coherent, the developed method can be used to determine the position of the ionospheric layer on beam trajectory *GTL*. The results of determining displacement *d* of the layers in intervals *a* and *b* are shown in Figs. 2-III and 2-IV. Here, curves *1*, *2*, and *3* represent the dependence of amplitudes A_a and A_p and displacement *d* on the altitude of the beam perigee, respectively. Curves *4* in Figs. 2-III and 2-IV indicate the angles of inclination of layers δ in degrees (vertical scales on the right). Curves *5* represent corrections Δh [km] to actual altitude h' of layer *a* (Fig. 2-III) and layer *b* (Fig. 2-IV), respectively. For layers in intervals *a* and *b*, the values of displacement *d* are concentrated in the ranges from −630 to −800 km and from −600 to −750 km, respectively (interval *c* is not shown). On average, the values of displacement *d* for the layers in intervals *a* and *b* are −730 and −620 km, respectively. The average value of displacement *d* for the layer in interval *c* is positive and equal to 620 km.

We briefly consider the accuracy of determining key characteristics (displacement and angle of inclination) of the sporadic layers using the radio occultation method. In accordance with Eq. (5), the statistical error in estimating the ratio $(A_a - A_p)/A_p$ will be minimal at maximum value A_p. Taking into account Eq. (5) and the fact that the experimental errors in determining A_p are < 5%, it can be shown that the accuracy of estimating *d* is no worse than ±100 km. This corresponds to an error of ~13%, when calculating the mean displacements for layers *a*, *b*, and *c* in this experiment. Since the errors in finding r_e are insignificant, it follows from Eq. (6) that the relative errors in determining the values of the angle of inclination ($\Delta\delta/\delta$) and the displacement ($\Delta d/d$) of the layers are approximately the same and equal to ~12–14%. Using Eq. (6), we found the values of the angle of inclination for plasma layers *a*, *b*, and *c* and the errors of their determination, which are $\delta = -7.3° \pm 0.9°$, $\delta = -6.4° \pm 0.9°$, and $\delta = 6.4° \pm 0.9°$, respectively. The values of correction Δh to actual altitude h' were also determined for layers *a* (Δh = 40 km), *b* (Δh = 30 km), and *c* (Δh = 30 km).

Local spherical symmetry allows us to apply the Abel transform to solve the inverse problem and find the distribution of electron density and its vertical gradient in the layer. The obtained dependence of the electron density $N_e(h')$ and the gradient dN_e/dh' are shown in Figs. 3 and 4, respectively. Altitude profiles of electron density and its vertical gradient for layers *a*, *b*, and *c* were reconstructed by us from radio occultation data on the eikonal. Actual layer altitude h' and the altitude of beam perigee *h* are shown on the top and bottom horizontal axes of Figs. 3 and 4, respectively. The altitude location of the electron density maxima coincides with the location of the refraction attenuation minima for layers *a*, *b*, and *c*, which can be easily seen from a comparison of Figs. 2-I and 3. This is fully consistent with the simulation results obtained in [52]. When the radio wave propagation vector is parallel to the ionization plane of the sporadic E-layer, then the radio beam transmission of the central part of the layer (peak of electron density) and its edges leads to defocusing and focusing of the beams, respectively [52]. Layers *a* and *b* are located on a segment of the *LT* beam at distances of 730 and 620 km from point *T*, in this case, their maximum electron density gradients are observed at altitudes of 95.0 and 114.5 km (Figs. 4a and 4b). Layer *c* is located at a distance of 620 km from point *T* on part of the *GT* beam with a maximum vertical gradient at the altitude of 130 km. According to Fig. 4, the values of the vertical gradient of electron density for layers *a*, *b*, and *c* are enclosed in the following intervals:

$$-3.0 \cdot 10^5 \text{ cm}^{-3}/\text{km} < dN_e(h')/dh' < 5.6 \cdot 10^5 \text{ cm}^{-3}/\text{km},$$

$$-2.4 \cdot 10^5 \text{ cm}^{-3}/\text{km} < dN_e(h')/dh' < 8.5 \cdot 10^5 \text{ cm}^{-3}/\text{km},$$

$$-1.7 \cdot 10^5 \text{ cm}^{-3}/\text{km} < dN_e(h')/dh' < 2.8 \cdot 10^5 \text{ cm}^{-3}/\text{km}.$$

These values are typical for intense sporadic E-layers in Earth's ionosphere observed using ground-based facilities of remote sensing, in situ methods, and satellite sensors [4, 35, 53]. The altitude range of variations in the amplitude of the radio occultation signal approximately corresponds to the range of variations in electron density and its vertical gradient.

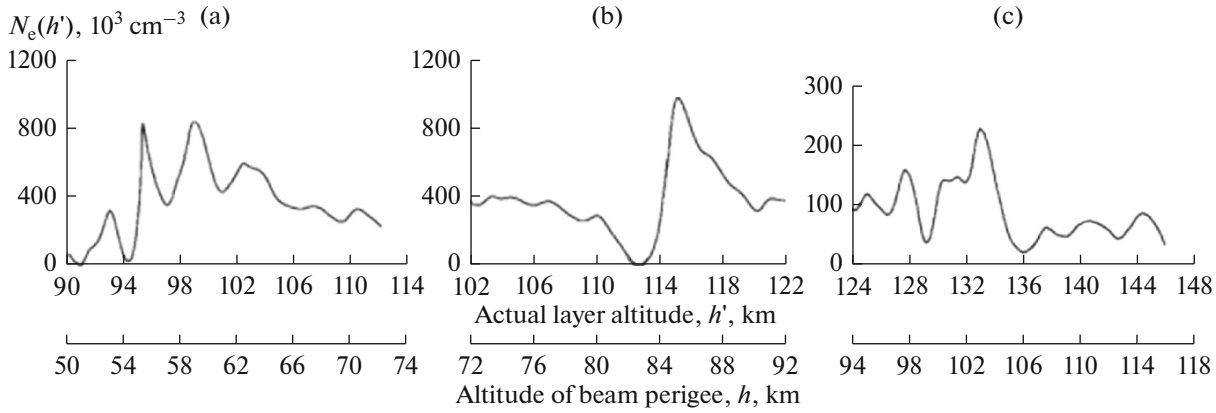

Fig. 3. Results of determining the electron density for three ionospheric layers. Displacement, altitude correction, and angle of inclination of the layer are equal, respectively: $d = -730$ km, $\Delta h = 40$ km, and $\delta = -7.3°$ (layer *a*, panel a); $d = -620$ km, $\Delta h = 30$ km, and $\delta = -6.4°$ (layer *b*, panel b); $d = 620$ km, $\Delta h = 30$ km, and $\delta = 6.4°$ (layer *c*, panel c).

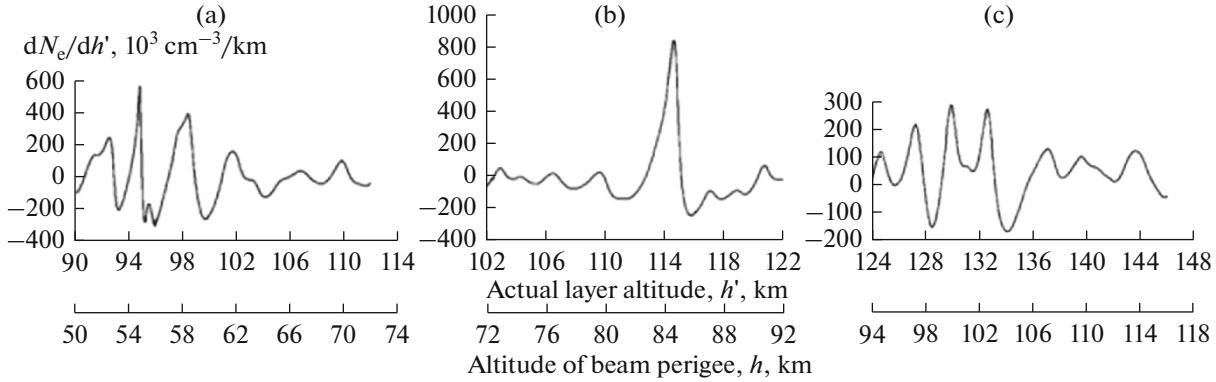

Fig. 4. Results of determining the vertical gradient of electron density for ionospheric layers.

4. ASSOCIATION BETWEEN INCLINED SPORADIC *E*-LAYERS AND INTERNAL ATMOSPHERIC WAVES

Propagation of IGWs at ionospheric altitudes of Earth can lead to the formation of inhomogeneities in ionization [54]. At present, it is known that internal atmospheric waves generate traveling ionospheric disturbances (TIDs) and some types of sporadic *E*-inhomogeneities. It was found that TIDs are characterized by a pronounced inclination of the equal phase surfaces, while almost horizontal equal phase surfaces are observed in sporadic *E*-layers. This is mainly due to the fact that sporadic layers are formed by atmospheric tides and buoyancy waves with a long period, which are destroyed in the *F*-region of the ionosphere due to dissipative effects [55]. According to the results in [54], the inclined fronts of TIDs should represent the phase fronts of the buoyancy waves associated with them, and the propagation of the wave phase downward indicates the propagation of the IGW energy upward. It should be noted that in [56] it was shown that polarization electric fields can be the cause of the appearance of medium scale TIDs. This is due to the fact that most nighttime TIDs are propagated in a southwestern direction, and this preferred direction of TID propagation cannot be explained by the classical theory of IGWs. The ionospheric instability, which acts through electrodynamic processes, including polarization electric fields, could also develop medium scale TIDs [56]. In [57], the association of sporadic *E*-layers with TIDs and other ionospheric phenomena was investigated.

An internal atmospheric wave propagating through the ionosphere collects ionization into a wave node due to collisions between charged and neutral particles. In [58], it was shown that a wave propagating through the *E*-region generates wave-like variations in electron density that have the same wave numbers and frequency as the initial IGW, provided there are no boundaries or inhomogeneities in the surrounding plasma. The authors in [59] have found that the wind shear tends to collect ionization into a wave node that is shifted down. This drift of ionization from higher levels to lower levels is known as the corkscrew effect.

The role of small-scale internal waves modulating the plasma layer formed by the tidal system was considered in [60]. The author of the above-mentioned paper indicated that in the case, when the vertical IGW phase velocity is slightly higher than the drift velocity of the plasma layer and is directed downward, the layer ions "see" the wind structure of the practically stationary IGW, which sweeps ions through the horizontal convergence/divergence zones, creating a characteristic "spottiness" of a sporadic *E*-layer. Forced spatial resonance arises, when the inhomogeneity in ionization formed in some other way (for example, by atmospheric tide or an IGW with a long period) has a drift velocity equal to the IGW phase velocity. In this case, the initial inhomogeneity should be located in such a way that it coincides with one of the ionization peaks created by an atmospheric wave [61].

Propagation of an internal atmospheric wave modulates the structure of the initially horizontal sporadic *E*-layer and leads to rotation of the plasma density gradient in the direction of its wave vector. Based on the fact that IGWs determine the angle of inclination of the sporadic *E*-layer by turning the plane of ionization of the layer parallel to its phase front, we have developed a new method for determining the characteristics of internal atmospheric waves associated with inclined sporadic structures in Earth's ionosphere. When reconstructing IGW parameters, we used the basic expressions (dispersion equation, polarization coupling relations, determinations of wave characteristics) for IGWs [62–68]. This method allows us to study the relationships between small-scale internal waves and sporadic *E*-layers in the Earth's ionosphere and significantly expands the capabilities of traditional radio occultation monitoring of the atmosphere [50].

The idea of experimental determination of the IGW characteristics associated with inclined plasma structures is as follows. A small-scale internal wave propagating through the *E*-region causes the inclination of the sporadic *E*-layer, turning its ionization plane parallel to the phase front of the internal wave. In this case, angle δ between the wave propagation vector and the local vertical will coincide with the angle of inclination of the plasma E_s-layer under study. To calculate characteristics of the IGWs which cause the slopes of the layers, it is necessary to have estimates of the unperturbed Brent–Väisälä frequency (N_b) at actual altitudes (h'), where sporadic layers *a*, *b*, and *c* are located. Since the data on the N_b value at the altitudes of the *E*-layers are rather conservative, we used the results obtained for Earth's reference atmosphere: $N_b(h' = 95\ \text{km}) \approx 2.3 \cdot 10^{-2}$ rad/s; $N_b(h' = 99\ \text{km}) \approx 2.2 \cdot 10^{-2}$ rad/s; $N_b(h' = 115\text{m}) \approx 2.1 \cdot 10^{-2}$ rad/s [55]. These values for buoyancy frequency N_b correspond to the values of the period τ_b ($\tau_b = 2\pi/N_b$) from 4.6 to 5.0 min, and they are consistent with the vertical profile of the buoyancy period τ_b calculated for the standard atmosphere, which is shown on p. 276 in [35] (see Fig. 6.5). From the results presented in Fig. 6.5 in [35], it was also determined that $N_b(h' = 133\ \text{km}) \approx 2.3 \cdot 10^{-2}$ rad/s. Using these estimates and the obtained experimental data, we found that: $1 \gg \tan^2\delta$ and $\omega^2 \gg f^2$. Considering the above inequalities, the dispersion equation and expressions for wave characteristics take the very simple form [50]:

$$\begin{gathered}\omega/N_b = \lambda_z/\lambda_h = |\tan\delta|, \quad \tau_i = 2\pi/\omega, \\ \left|c_{ph}^{\text{in}}\right| = \omega/|k_h| = N_b/|m|, \\ \left|c_{pz}^{\text{in}}\right| = \omega/|m| = N_b|\tan\delta|/|m|,\end{gathered} \tag{7}$$

where ω is the IGW intrinsic frequency; τ_i is the intrinsic period of the internal wave; $k_h = 2\pi/\lambda_h$ and $m = 2\pi/\lambda_z$ are the horizontal and vertical wave numbers; λ_h and λ_z are the horizontal and vertical wavelengths; c_{ph}^{in} and c_{pz}^{in} are intrinsic horizontal and vertical phase velocities. Based on relations (7), it is possible to calculate the characteristics of small-scale internal waves, which cause the inclinations of the initially horizontal sporadic *E*-layers in Earth's ionosphere:

Layer *a* (bottom) ($h' = 95$ km, $\Delta h = 40$ km): $\lambda_z = 3.0$ km; $\delta = -7.3°$; $|\tan\delta| = 0.13$; $\lambda_h = 23.1$ km; $\left|c_{ph}^{\text{in}}\right| = 11.0$ m/s; $\left|c_{pz}^{\text{in}}\right| = 1.4$ m/s; $N_b = 2.3 \cdot 10^{-2}$ rad/s; $\omega = 3.0 \cdot 10^{-3}$ rad/s; and $\tau_i = 34.9$ min.

Layer *a* (top) ($h' = 99$ km, $\Delta h = 40$ km): $\lambda_z = 4.4$ km; $\delta = -7.3°$; $|\tan\delta| = 0.13$; $\lambda_h = 33.8$ km; $\left|c_{ph}^{\text{in}}\right| = 15.4$ m/s; $\left|c_{pz}^{\text{in}}\right| = 2.0$ m/s; $N_b = 2.2 \cdot 10^{-2}$ rad/s; $\omega = 2.9 \cdot 10^{-3}$ rad/s; and $\tau_i = 36.1$ min.

Layer *b* ($h' = 115$ km, $\Delta h = 30$ km): $\lambda_z = 4.4$ km; $\delta = -6.4°$; $|\tan\delta| = 0.11$; $\lambda_h = 40.0$ km; $\left|c_{ph}^{\text{in}}\right| = 14.7$ m/s; $\left|c_{pz}^{\text{in}}\right| = 1.6$ m/s; $N_b = 2.1 \cdot 10^{-2}$ rad/s; $\omega = 2.3 \cdot 10^{-3}$ rad/s; and $\tau_i = 45.5$ min.

Layer *c* ($h' = 133$ km, $\Delta h = 30$ km): $\lambda_z = 3.0$ km; $\delta = 6.4°$; $|\tan\delta| = 0.11$; $\lambda_h = 27.3$ km; $\left|c_{ph}^{\text{in}}\right| = 11.0$ m/s; $\left|c_{pz}^{\text{in}}\right| = 1.2$ m/s; $N_b = 2.3 \cdot 10^{-2}$ rad/s; $\omega = 2.5 \cdot 10^{-3}$ rad/s; and $\tau_i = 41.9$ min.

We briefly consider the reconstruction errors of the above-mentioned characteristics of small-scale atmospheric waves modulating sporadic layers. Earlier in Section 3, we estimated the relative error in determining the angles of inclination δ (and $|\tan\delta|$) for layers *a*, *b*, and *c* as ~12–14%. Assuming that the errors in determining N_b from profiles for Earth's reference atmosphere do not exceed ~5%, using the first two relations in (7), we can find the relative errors in calculating intrinsic frequency ω and period τ_i of internal waves: ~13–15%. If the accuracy of the experimental estimate of λ_z is ~5%, then the errors in determining

horizontal wavelength λ_h will also be ~13–15%. Using the third and fourth relations in (7) and the above-mentioned errors in determining N_b, λ_z, and ω, we find that the errors in calculating the intrinsic horizontal c_{ph}^{in} and vertical c_{pz}^{in} phase velocities are ~7 and ~14–16%, respectively.

It is important that the value of the intrinsic frequency and the IGW period can be determined by knowing only the values of the Brent–Väisälä frequency (N_b) and angle (δ) between the wave propagation vector and the local vertical. The intrinsic period of the studied internal waves is from 35 to 46 min, and the values of the IGW intrinsic vertical phase velocity are in the range from 1.2 to 2.0 m/s. The indicated estimates are in good agreement with an ~30 min period and a vertical wind velocity <2.0 m/s at an altitude of ~100 km (in the ground-based reference system) calculated for the sporadic *E*-layer model in the polar cap [69, 70]. It should be noted that the nodes of the wind shear, in which the wind velocity is equal to zero, coincide with the location of the E_s-layers, therefore, the intrinsic wave period must coincide with the IGW period in the ground-based system [66]. Thus, intrinsic periods of waves τ_i from 35 to 46 min fully correspond to the results in the ground-based system obtained in studies of Earth's high-latitude ionosphere [37, 45, 69–71].

CONCLUSIONS

A method has been developed for determining the characteristics of internal atmospheric waves based on the use of inclined sporadic *E*-layers of the ionosphere as a detector. The method is based on the fact that an internal wave propagating through an initially horizontal sporadic *E*-layer leads to rotation of the plasma density gradient in the direction of the wave vector and to turning the ionization plane of the layer parallel to the phase front of the wave. The developed method allows us to study the relationships between small-scale internal waves and sporadic *E*-layers in Earth's ionosphere and significantly expands the capabilities of traditional radio occultation monitoring of the atmosphere. It was found that the studied atmospheric waves have periods from 35 to 46 min and vertical phase velocities from 1.2 to 2.0 m/s, which is in good agreement with the results of independent experiments and modeling data for sporadic *E*-structures at an altitude of ~100 km in Earth's polar cap.

FUNDING

This study was supported by a state task and was partially supported by the Russian Foundation for Basic Research (RFBR project no. 19-02-00083 A) and program no. 12 of the Presidium of the Russian Academy of Sciences.

REFERENCES

1. Wu, D.L., Ao, C.O., Hajj, G.A., de la Torre Juarez, M., et al., Sporadic *E* morphology from GPS-CHAMP radio occultations, *J. Geophys. Res.*, 2005, vol. 110, A01306. https://doi.org/10.1029/2004JA010701
2. Arras, C., Wickert, J., Beyerle, G., et al., A global climatology of ionospheric irregularities derived from GPS radio occultation, *Geophys. Res. Lett.*, 2008, vol. 35, L14809. https://doi.org/10.1029/2008GL03415
3. Haldoupis, C.A., Tutorial review on sporadic *E* layers, in *Aeronomy of the Earth's Atmosphere and Ionosphere*, Abdu, M.A., Pancheva, D., and Bhattacharyya, A., Eds., Berlin: Springer, 2011, pp. 381–394. https://doi.org/10.1007/978-94-007-0326-1-2
4. Whitehead, J.D., Recent work on midlatitude and equatorial sporadic E, *J. Atmos. Terr. Phys.*, 1989, vol. 51, pp. 401–424. https://doi.org/10.1016/0021-9169(89)90122-0
5. Kirkwood, S. and Nilsson, H., High-latitude sporadic-E and other thin layers—the role of magnetospheric electric fields, *Space Sci. Rev.*, 2000, vol. 91, pp. 579–613.
6. Haldoupis, C., Midlatitude sporadic E layers. A typical paradigm of atmosphere–ionosphere coupling, *Space Sci. Rev.*, 2012, vol. 168, pp. 441–461.
7. Roddy, P.A., Earle, G.D., Swenson, C.M., et al., Relative concentrations of molecular and metallic ions in midlatitude intermediate and sporadic-E layers, *Geophys. Res. Lett.*, 2004, vol. 31, L19807. https://doi.org/10.1029/2004GL020604
8. Maruyama, T., Kato, H., and Nakamura, M., Ionospheric effects of the Leonid meteor shower in November 2001 as observed by rapid run ionosondes, *J. Geophys. Res.*, 2003, vol. 108, no. A8, 1324. https://doi.org/10.1029/2003JA009831
9. Maruyama, T., Kato, H., and Nakamura, M., Meteor-induced transient sporadic E as inferred from rapid-run ionosonde observations at midlatitudes, *J. Geophys. Res.*, 2008, vol. 113, A09308. https://doi.org/10.1029/2008JA013362
10. Malhotra, A., Mathews, J.D., and Urbina, J., Effect of meteor ionization on sporadic-E observed at Jicamarca, *Geophys. Res. Lett.*, 2008, vol. 35, L15106. https://doi.org/10.1029/2008GL034661
11. Hysell, D.L., Yamamoto, M., and Fukao, S., Imaging radar observations and theory of type I and type II quasi-periodic echoes, *J. Geophys. Res.*, 2002, vol. 107, no. A11, 1360. https://doi.org/10.1029/2002JA009292
12. Hysell, D.L., Larsen, M.F., and Zhou, Q.H., Common volume coherent and incoherent scatter radar observations of mid-latitude sporadic E-layers and QP echoes, *Ann. Geophys.*, 2004, vol. 22, pp. 3277–3290. https://doi.org/10.5194/angeo-22-3277-2004
13. Larsen, M.F., Hysell, D.L., Zhou, Q.H., et al., Imaging coherent scatter radar, incoherent scatter radar, and optical observations of quasiperiodic structures associated with sporadic E layers, *J. Geophys. Res.*, 2007, vol. 112, A06321. https://doi.org/10.1029/2006JA012051
14. Cosgrove, R.B. and Tsunoda, R.T., A direction-dependent instability of sporadic-E layers in the nighttime midlatitude ionosphere, *Geophys. Res. Lett.*, 2002,

vol. 29, no. 18, 1864.
https://doi.org/10.1029/2002GL014669

15. Cosgrove, R.B. and Tsunoda, R.T., Instability of the E–F coupled nighttime midlatitude ionosphere, *J. Geophys. Res.*, 2004, vol. 109, A04305.
https://doi.org/10.1029/2003JA010243
16. Yokoyama, T., Hysell, D.L., Otsuka, Y., and Yamamoto, M., Three-dimensional simulation of the coupled Perkins and ES-layer instabilities in the nighttime midlatitude ionosphere, *J. Geophys. Res.*, 2009, vol. 114, A03308.
https://doi.org/10.1029/2008JA013789
17. Woodman, R.F., Yamamoto, M., and Fukao, S., Gravity wave modulation of gradient drift instabilities in mid-latitude sporadic E irregularities, *Geophys. Res. Lett.*, 1991, vol. 18, pp. 1197–1200.
https://doi.org/10.1029/91GL01159
18. Didebulidze, G.G. and Lomidze, L.N., Double atmospheric gravity wave frequency oscillations of sporadic E formed in a horizontal shear flow, *Phys. Lett. A*, 2010, vol. 374, no. 7, pp. 952–969.
19. Chu, Y.-H., Brahmanandam, P.S., Wang, C.-Y., et al., Coordinated sporadic E layer observations made with Chung-Li 30 MHz radar, ionosonde and FORMOSAT-3/COSMIC satellites, *J. Atmos. Sol.-Terr. Phys.*, 2011, vol. 73, pp. 883–894.
20. Larsen, M.F., A shear instability seeding mechanism for quasiperiodic radar echoes, *J. Geophys. Res.*, 2000, vol. 105, no. A11, pp. 24931–24940.
https://doi.org/10.1029/1999JA000290
21. Bernhardt, P.A., The modulation of sporadic-E layers by Kelvin–Helmholtz billows in the neutral atmosphere, *J. Atmos. Sol.-Terr. Phys.*, 2002, vol. 64, pp. 1487–1504.
22. Hysell, D.L., Nossa, E., Larsen, M.F., et al., Sporadic E layer observations over Arecibo using coherent and incoherent scatter radar: Assessing dynamic stability in the lower thermosphere, *J. Geophys. Res.*, 2009, vol. 114, A12303.
https://doi.org/10.1029/2009JA014403
23. Tsunoda, R.T., Fukao, S., and Yamamoto, M., On the origin of quasiperiodic radar backscatter from midlatitude sporadic E, *Radio Sci.*, 1994, vol. 29, pp. 349–366.
24. Yamamoto, M., Fukao, S., Woodman, R.F., et al., Mid-latitude e region field-aligned irregularities observed with the MU radar, *J. Geophys. Res.: Space*, 1991, vol. 96, pp. 15943–15949.
25. Yamamoto, M., Fukao, S., Ogawa, T., et al., A morphological study of mid-latitude *E*-region field-aligned irregularities observed with the MU radar, *J. Atmos. Sol.-Terr. Phys.*, 1992, vol. 54, pp. 769–777.
26. Bernhardt, P.A., Selcher, C.A., Siefring, C., et al., Radio tomographic imaging of sporadic-E layers during SEEK-2, *Ann. Geophys.*, 2005, vol. 23, pp. 2357–2368.
https://doi.org/10.5194/angeo-23-2357-2005
27. Yamamoto, M., Fukao, S., Tsunoda, R.T., et al., SEEK-2 (Sporadic-*E* Experiment over Kyushu 2)—project outline, and significance, *Ann. Geophys.*, 2005, vol. 23, pp. 2295–2305.
https://doi.org/10.5194/angeo-23-2295-2005
28. Larsen, M.F., Fukao, S., Yamamoto, M., et al., The SEEK chemical release experiment: Observed neutral wind profile in a region of sporadic-E, *Geophys. Res. Lett.*, 1998, vol. 25, pp. 1789–1792.
29. Larsen, M.F., Yamamoto, M., Fukao, S., and Tsunoda, R.T., SEEK 2: Observations of neutral winds, wind shears, and wave structure during a sporadic E/QP event, *Ann. Geophys.*, 2005, vol. 23, pp. 2369–2375.
30. Yokoyama, T., Yamamoto, M., Fukao, S., et al., Numerical simulation of mid-latitude ionospheric *E*-region based on SEEK and SEEK-2 observations, *Ann. Geophys.*, 2005, vol. 23, no. 7, pp. 2377–2384.
31. Saito, S., Yamamoto, M., Hashiguchi, H., and Maegawa, A., Observation of three-dimensional structures of quasi-periodic echoes associated with mid-latitude sporadic-E layers by MU radar ultra-multi-channel system, *Geophys. Res. Lett.*, 2006, vol. 33, L14109.
https://doi.org/10.1029/2005GL025526
32. Maruyama, T., Fukao, S., and Yamamoto, M., A possible mechanism for echo striation generation of radar backscatter from midlatitude sporadic E, *Radio Sci.*, 2000, vol. 35, pp. 1155–1164.
33. Ogawa, T., Takahashi, O., Otsuka, Y., et al., Simultaneous middle and upper atmosphere radar and ionospheric sounder observations of midlatitude E region irregularities and sporadic E layer, *J. Geophys. Res.*, 2002, vol. 107, no. A10, 1275.
https://doi.org/10.1029/2001JA900176
34. Yokoyama, T., Yamamoto, M., Fukao, S., and Cosgrove, R.B., Three-dimensional simulation on generation of polarization electric field in the midlatitude E-region ionosphere, *J. Geophys. Res.*, 2004, vol. 109, A01309.
https://doi.org/10.1029/2003JA010238
35. Kelley, M.C., *The Earth's Ionosphere: Plasma Physics and Electrodynamics*, San Diego, Calif.: Academic Press, 2009.
36. Nygren, T., Jalonen, L., Oksman, J., and Turunen, T., The role of electric field and neutral wind direction in the formation of sporadic E-layers, *J. Atmos. Terr. Phys.*, 1984, vol. 46, pp. 373–381.
37. Turunen, T., Nygren, T., and Huuskonen, A., Nocturnal high-latitude E-region in winter during extremely quiet conditions, *J. Atmos. Terr. Phys.*, 1993, vol. 55, pp. 783–795.
38. Bristow, W.A. and Watkins, B.J., Numerical simulation of the formation of thin ionization layers at high latitudes, *Geophys. Res. Lett.*, 1991, vol. 18, pp. 404–407.
39. Bristow, W.A. and Watkins, B.J., Incoherent scatter observations of thin ionization layers at Sondrestrom, *J. Atmos. Terr. Phys.*, 1993, vol. 55, pp. 873–894.
40. Kirkwood, S. and von Zahn, U., On the role of auroral electric fields in the formation of low altitude sporadic-E and sudden sodium layers, *J. Atmos. Terr. Phys.*, 1991, vol. 53, pp. 389–407.
41. Kirkwood, S. and von Zahn, U., Formation mechanisms for lowaltitude Es and their relationship with neutral Fe layers: Results from the metal campaign, *J. Geophys. Res.*, 1993, vol. 98, pp. 21549–21561.
42. Lehmacher, G.A., Larsen, M.F., and Croskey, C.L., Observation of electron biteout regions below sporadic E layers at polar latitudes, *Ann. Geophys.*, 2015, vol. 33, pp. 371–380.
https://doi.org/10.5194/angeo-33-371-2015
43. Cox, R.M. and Plane, J.M.C., An ion–molecule mechanism for the formation of neutral sporadic Na layers, *J. Geophys. Res.*, 1998, vol. 103, no. D6, pp. 6349–6359.

44. Hunten, D.M., Turco, R.P., and Toon, O.B., Smoke and dust particles of meteoric origin in the mesosphere and stratosphere, *J. Atmos. Sci.*, 1980, vol. 37, pp. 1342–1357.
45. Heinselman, C.J., Thayer, J.P., and Watkins, B.J., A high-latitude observation of sporadic sodium and sporadic E-layer formation, *Geophys. Res. Lett.*, 1998, vol. 25, pp. 3059–3062.
46. Igarashi, K., Pavelyev, A.G., Hocke, K., et al., Observation of wave structures in the upper atmosphere by means of radio holographic analysis of the RO data, *Adv. Space Res.*, 2001, vol. 27, pp. 1321–1327.
47. Pavelyev, A.G., Liou, Y.A., Wickert, J., et al., New applications and advances of the GPS radio occultation technology as recovered by analysis of the FORMOSAT-3/COSMIC and CHAMP data-base, in New Horizons in *Occultation Research: Studies in Atmosphere and Climate*, Steiner, A., Pirscher, B., Foelsche, U., and Kirchengast, G., Eds., Berlin–Heidelberg: Springer, 2009.
https://doi.org/10.1007/978-3-642-00321_9
48. Pavelyev, A.G., Liou, Y.A., Zhang, K., et al., Identification and localization of layers in the ionosphere using the eikonal and amplitude of radio occultation signals, *Atmos. Meas. Tech*., 2012, vol. 5, no. 1, pp. 1–16.
https://doi.org/10.5194/amt-5-1-2012
49. Pavelyev, A.G., Liou, Y.A., Matyugov, S.S., et al., Application of the locality principle to radio occultation studies of the Earth's atmosphere and ionosphere, *Atmos. Meas. Tech*., 2015, vol. 8, no. 7, pp. 2885–2899.
https://doi.org/10.5194/amt-8-2885-2015
50. Gubenko, V.N., Pavelyev, A.G., Kirillovich, I.A., and Liou, Y.-A., Case study of inclined sporadic E layers in the Earth's ionosphere observed by CHAMP/GPS radio occultations: Coupling between the tilted plasma layers and internal waves, *Adv. Space Res.*, 2018, vol. 61, no. 7, pp. 1702–1716.
https://doi.org/10.1016/j.asr.2017.10.001
51. Yue, X., Schreiner, W.S., Zeng, Z., et al., Case study on complex sporadic E layers observed by GPS radio occultations, *Atmos. Meas. Tech*., 2015, vol. 8, pp. 225–236.
https://doi.org/10.5194/amt-8-225-2015
52. Zeng, Z. and Sokolovskiy, S., Effect of sporadic E cloud on GPS radio occultation signal, *Geophys. Res. Lett.*, 2010, vol. 37, L18817.
https://doi.org/10.1029/2010GL044561
53. Mathews, J.D., Sporadic E: Current views and recent progress, *J. Atmos. Sol.-Terr. Phys.*, 1998, vol. 60, no. 4, pp. 413–435.
https://doi.org/10.1016/S1364-6826(97)00043-6
54. Hines, C.O., Internal atmospheric gravity waves at ionospheric heights, *Can. J. Phys.*, 1960, vol. 38, pp. 1441–1481.
55. Gossard, E.E. and Hooke, W.H., *Waves in the Atmosphere*, Amsterdam–Oxford–New York: Elsevier, 1975.
56. Otsuka, Y., Shiokawa, K., Ogawa, T., et al., Spatial relationship of nighttime medium-scale traveling ionospheric disturbances and f region field-aligned irregularities observed with two spaced all-sky airglow imagers and the middle and upper atmosphere radar, *J. Geophys. Res.*, 2009, vol. 114, A05302.
https://doi.org/10.1029/2008JA013902
57. Tsunoda, R.T. and Cosgrove, R.B., Coupled electrodynamics in the nighttime midlatitude ionosphere, *Geophys. Res. Lett.*, 2001, vol. 8, pp. 4171–4174.
58. Kato, S., Reddy, C.A., and Matsushita, S., Possible hydromagnetic coupling between the perturbations of the neutral and ionized atmosphere, *J. Geophys. Res.*, 1970, vol. 75, pp. 2540–2550.
59. Chimonas, G. and Axford, W.I., Vertical movement of temperate-zone sporadic E layers, *J. Geophys. Res.*, 1968, vol. 73, pp. 111–117.
60. Chimonas, G., Enhancement of sporadic *E* by horizontal transport within the layer, *J. Geophys. Res.*, 1971, vol. 76, pp. 4578–4586.
61. Whitehead, J.D., Ionization disturbances caused by gravity waves in the presence of an electrostatic field and background wind, *J. Geophys. Res.*, 1971, vol. 76, pp. 238–241.
62. Gubenko, V.N., Pavelyev, A.G., and Andreev, V.E., Determination of the intrinsic frequency and other wave parameters from a single vertical temperature or density profile measurement, *J. Geophys. Res.*, 2008, vol. 113, D08109.
https://doi.org/10.1029/2007JD008920
63. Gubenko, V.N., Pavelyev, A.G., Salimzyanov, R.R., and Pavelyev, A.A., Reconstruction of internal gravity wave parameters from radio occultation retrievals of vertical temperature profiles in the Earth's atmosphere, *Atmos. Meas. Tech*., 2011, vol. 4, no. 10, pp. 2153–2162.
https://doi.org/10.5194/amt-4-2153-2011
64. Gubenko, V.N., Pavelyev, A.G., Salimzyanov, R.R., and Andreev, V.E., A method for determination of internal gravity wave parameters from a vertical temperature or density profile measurement in the Earth's atmosphere, *Cosmic Res.*, 2012, vol. 50, no. 1, pp. 21–31.
65. Gubenko, V.N., Kirillovich, I.A., and Pavelyev A.G. Characteristics of internal waves in the Martian atmosphere obtained on the basis of an analysis of vertical temperature profiles of the *Mars Global Surveyor* mission, *Cosmic Res.*, 2015, vol. 53, no. 2, pp. 133–142.
https://doi.org/10.1134/S0010952515020021
66. Gubenko, V.N. and Kirillovich, I.A., Diagnostics of internal atmospheric wave saturation and determination of their characteristics in Earth's stratosphere from radiosonde measurements, *Sol.-Terr. Phys.*, 2018, vol. 4, no. 2, pp. 41–48.
https://doi.org/10.12737/stp-42201807
67. Gubenko, V.N., Kirillovich, I.A., Pavelyev, A.G., and Andreev, V.E., Detection of saturated internal gravity waves in the Martian atmosphere and reconstruction of their characteristics, *Izv. Vyssh. Uchebn. Zaved., Fiz.*, 2016, vol. 59, no. 12-2, pp. 46–49.
68. Gubenko, V.N., Kirillovich, I.A., Liou, I.-A., and Pavelyev, A.G., Monitoring of the activity of internal gravity waves in the atmosphere of the Arctic and Antarctic, *Izv. Vyssh. Uchebn. Zaved., Fiz.*, 2016, vol. 59, no. 12-3, pp. 80–85.
69. MacDougall, J.W., Jayachandran, P.T., and Plane, J.M.C., Polar cap sporadic-E: Part 1. Observations, *J. Atmos. Sol.-Terr. Phys.*, 2000, vol. 62, pp. 1155–1167.
70. MacDougall, J.W., Plane, J.M.C., and Jayachandran, P.T., Polar cap sporadic-E: Part 2. Modeling, *J. Atmos. Sol.-Terr. Phys.*, 2000, vol. 62, pp. 1169–1176.
71. Kirkwood, S. and Collis, P.N., Gravity wave generation of simultaneous auroral sporadic-E layers and sudden neutral sodium layers, *J. Atmos. Terr. Phys.*, 1989, vol. 51, no. 4, pp. 259–269.

Translated by N. Topchiev